Micropatterning of Organic Electronic Devices by Cold-Welding

Changsoon Kim, Paul E. Burrows, Stephen R. Forrest*

A simple and general postdeposition electrode patterning technique for active organic electronic devices is demonstrated and is applied to patterning the metal cathodes of organic light-emitting devices. Selective lift-off of the metal cathode layer is achieved by pressing a prepatterned, metal-coated silicon stamp on the unpatterned device layers. Under pressure, the metal coating on the stamp cold-welds to the metal cathode coating the underlying organic films. Subsequent separation of the stamp from the substrate results in removal of the cathode metal in the regions contacted by the stamp, resulting in submicrometer feature definition. A 17×17 passive matrix display, with a pixel size of 440 micrometers by 320 micrometers, was fabricated with this process. Cold-welding followed by lift-off of the cathode metal allows simple, cost-effective, and high-throughput large-area fabrication of organic electronic devices.

A significant limitation to the realization of advanced organic electronic devices is the lack of a simple and low-cost means for patterning of fragile organic thin films. The use of conventional photoresist processing used in inorganic device patterning is difficult, because many organic materials degrade when exposed to solvents or aqueous chemicals. Given the low electrical conductivity of most organic thin films, contact patterning alone is generally sufficient to define the device. Attention has, therefore, been focused primarily on using shadow-mask techniques (1) to pattern the contact regions of the devices. Such a mask must be sufficiently thick to provide mechanical strength, thus ultimately limiting the pattern resolution. Several alternative patterning methods have also been demonstrated: use of an in situ photoresist shadow mask (2), excimer laser ablation (3), ink-jet printing (4–6), photolithographic undercut formation (7), "dry-film lift-off" (8), and conformal masking using elastomeric membranes (9). Here, we describe a technique for the direct micropatterning of active organic electronic devices by postdeposition, high-pressure stamping, which induces cold-welding between a metal coating on the stamp and the metal layer on the organic film, allowing removal of unwanted material. The advantages of this method are its capabilities for generating device patterns on a micrometer scale, using a simple, rapid, and nondestructive process. We demonstrated the fabrication of small molecular weight, vacuum-deposited or-

ganic light-emitting device (OLED) arrays with pattern sizes as small as 12 μm and submicrometer feature resolutions.

When two clean metal surfaces are brought into contact, an intimate metallic junction can be formed between the surfaces. When the interfacial separation of two atomically flat surfaces with similar orientations becomes comparable to the bulk interatomic distance, adhesion between the two surfaces becomes possible, eliminating the original interfacial separation (10, 11). In practice, however, the two surfaces are not atomically flat and may be coated with adsorbed molecules of oxygen, water vapor, oxide films, and other contamination. Thus, to produce an intimate metallic bond, it is necessary to apply considerable pressure across the interface to overcome the effects of these surface imperfections. This method of metallic bond formation is known as "cold-welding" (12, 13), a process we used to selectively lift off the metal cathode layers of organic optoelectronic devices. In particular, we used this technique to fabricate a display of high-performance OLEDs, although cold-welding followed by lift-off is sufficiently general that it can be used to form contacts on a broad range of organic devices, such as thin-film transistors and photovoltaic cells.

In the patterning process (Fig. 1), a prepatterned, metal-coated stamp composed of a rigid material such as Si is pressed onto an unpatterned film consisting of the organic device layers coated with the same metal contact layer as that used to coat the stamp. Typically, the total organic layer thickness is ~100 nm, with a similar thickness for the metal cathode. When a sufficiently high pressure is applied, an intimate metallic junction is formed between the metal layers on the stamp and the film, leading to a cold-welded bond (Fig. 1A, top). To induce

selective lift-off, additional pressure is applied to weaken the metal film at the edge of the stamp (Fig. 1A, middle). This additional pressure leads to substrate deformation, which is expected to enhance the local weakening of the metal film. When the stamp and film are separated, the metal cathode breaks sharply, forming a well-defined patterned electrode (Fig. 1A, bottom).

To estimate the stress distribution under pressure and to provide a semiquantitative understanding of the breakage process, we consider two elastic bodies in contact: the glass substrate and Si stamp. The presence of the multilayer between these two bodies, i.e. organic, metal, and indium tin oxide (ITO) films, is modeled by a single effective coefficient of friction (μ). We consider an infinitely long stamp with finite width ($2a$) and a thick glass substrate. With these assumptions, we calculate the normal stress at the surface (σ_{yy}) as a function of lateral position ($0 < x < a$) as measured from the center of the stamp, following the treatment of Spence (14). The lateral surface displacement of the glass material relative to the stamp is zero over the region $0 < x < c$ (adhesive region). For $c < x < a$, the finite μ
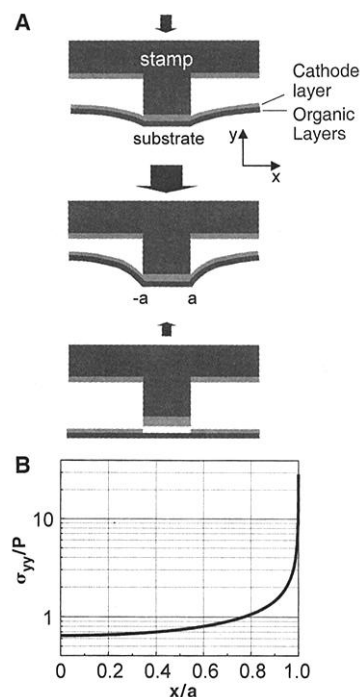

Fig. 1. (A) Schematic illustration of the direct micropatterning process by cold-welding followed by lift-off: (top) cold-welding occurs; (middle) a further increase of pressure results in substrate deformation, inducing weakening of the cathode layer along the stamp edge; (bottom) upon separation, selective lift-off of the metal cathode is achieved. **(B)** Calculated normal stress at the interface (σ_{yy}) normalized to the applied pressure (P) as a function of distance (x) normalized to the stamp half-width (a), using parameters in the text. The mesh size used for the calculation is $\delta/a = 10^{-3}$.

Center for Photonics and Optoelectronic Materials (POEM), Department of Electrical Engineering, and the Princeton Materials Institute, Princeton University, Princeton, NJ 08544, USA.

*To whom correspondence should be addressed. E-mail: forrest@ee.princeton.edu

allows for inward displacement of the glass material relative to the stamp. For Si, we use $E = 130$ GPa, $G = 51$ GPa, and $\nu = 0.278$ where E, G, and ν are the Young's modulus, shear modulus, and the Poisson ratio, respectively (15). For glass, $E = 70$ GPa, $G = 30$ GPa, and $\nu = 0.21$ are used (16). Now, σ_{yy} normalized to the applied pressure (P) is calculated (Fig. 1B) as a function of the normalized lateral position (x/a), assuming $\mu = 0.3$. We expect that μ for our model is larger than 0.3, since the coefficient of friction for the Ag-Ag contact is ~1 (12, 17). However, the normal stress distribution for $\mu \geq 0.3$ is very insensitive to μ, and is essentially the same as in the case of full adhesion ($\mu = \infty$, $C/a = 1$). Figure 1B shows a high concentration of stress near the periphery of the stamp. Considering the large applied pressures used in the experiments (>100 MPa), we conclude that the cathode layer near the edge is expected to be substantially plastically deformed and thus weakened. As a result, fracture along the boundaries occurs upon separation of the stamp from the film surface.

We applied this technique to the fabrication of conventional small-molecule OLEDs, using the following procedure: Before organic thin film and metal electrode deposition, a 13 mm by 13 mm by 1 mm glass substrate precoated with a ~1500 Å thick, transparent, conductive (20 ohms per square) ITO anode was cleaned (1), followed by exposure for 2 min in an oxygen plasma. The organic single heterostructure consisted of a 500 Å thick hole transport layer of 4,4'-bis[N-(1-napthyl)-N-phenyl-amino] biphenyl (α-NPD), followed by a 500 Å thick electron transport and light-emitting layer of tris-(8-hydroxyquinoline) aluminum (Alq$_3$). The cathode consisted of a 500 Å thick Mg:Ag alloy cathode capped with a 400 Å thick Ag layer. The stamps consisted of a Si wafer photolithographically patterned with raised areas in the shape of the regions on the OLED electrode that were to be removed. The pattern was formed by chlorine-based reactive ion etching or by wet etching (in 0.07:0.7:0.23 HF:HNO$_3$:CH$_3$COOH) to a depth of ~10 μm, using a SiO$_2$ mask. This depth was chosen to prevent possible unintentional contact of the stamp to the cathode layer due to the deformation of the glass substrate. The metal coating on the stamp, consisting of a 50 Å Cr adhesion layer followed by a 150 Å layer of Ag, was deposited by conventional electron-beam evaporation. Immediately following organic and electrode deposition, the stamp was pressed onto the unpatterned OLEDs, using an Instron Dynamic Testing System (model 8501), which applies force through a computer-controlled actuator. The substrate and stamp were placed on a cylinder-shaped platen, and compressive force was applied by moving the platen toward a fixed upper platen with the applied force increased linearly from zero to maximum. The

patterning of the OLEDs was done under ambient laboratory conditions; hence, neither the stamps nor the OLEDs were protected from dust, oxygen, water vapor, or other contaminants. It is anticipated that considerably lower pressures than those used by us can be applied to softer substrates or surfaces which are pressed immediately following deposition in a nonoxidizing, contamination-free environment.

Figure 2 shows a patterned array of 230-μm-diameter dots and the edge of a 12-μm-wide stripe pattern formed at a maximum pressure of 290 MPa and a ramp rate of 8 MPa/s. The pressure was released immediately after the maximum pressure was reached. The yield of this patterning process is high (Fig. 2A), with two defects (indicated by arrows) resulting from corresponding features on the stamp. We observed that the organic materials were also removed in some irregularly distributed areas between contacts. However, because these regions are between active devices, this partial removal should not cause a problem in device performance. Indeed, we subsequently exposed samples to an oxygen plasma after lift-off was completed in order to remove all residual organics between the metal, thus allowing for subsequent deposition and patterning. An atomic force microscope (AFM) scan across the metal edge (Fig. 2C) shows that the step edge abruptness is <150 nm, which is probably limited by the pattern definition of the stamp itself, thus setting an upper limit to the minimum feature size attainable with this process.

The operating characteristics of cold-weld–processed, 1-mm-diameter OLEDs are compared (Fig. 3) with those of similar devices patterned using conventional shadow-mask techniques. We note that both the current-voltage and quantum efficiency characteristics of both sets of devices are identical, to within experimental error. These undoped Alq$_3$ emitter devices have an "operating voltage" at 10 mA/cm^2 of $V_{10} = (5.1 \pm 0.1)$V, and an external quantum efficiency of $0.7 \pm 0.1\%$, depending on the current. These results are comparable to those of the best undoped Alq$_3$ devices of similar structure reported in the literature (18, 19) and indicate that there is no apparent degradation in performance incurred during the cathode patterning process.

To demonstrate a practical device with a prepatterned (not flat) substrate, we fabricated a 17×17 monochrome passive matrix array of 440 μm by 320 μm pixels with spacings of 190 μm between rows and 80 μm between columns. First, parallel lines consisting of a 1500 Å thick layer of predeposited, clean ITO on glass were patterned by a combination of conventional photolithography and wet etching to form the pixel rows. To prevent possible short circuits between the ITO and metal layers, a 1000 Å thick SiO$_2$ layer was deposited onto the substrate surface by plasma-enhanced chemical

vapor deposition, and then was patterned (Fig. 4A, inset). Next, a α-NPD and Alq$_3$ (thickness of both layers: 500 Å) organic heterostructure was deposited, followed by the full surface deposition of the Mg:Ag contact following the same process described above. A Si stamp with a parallel column line pattern was pressed onto the substrate with the column axis perpendicular to the prepatterned ITO rows (Fig. 4A). Figure 4B shows an intersection between the metal and the ITO lines, indicated by a small rectangle in Fig. 4A. The patterning is well
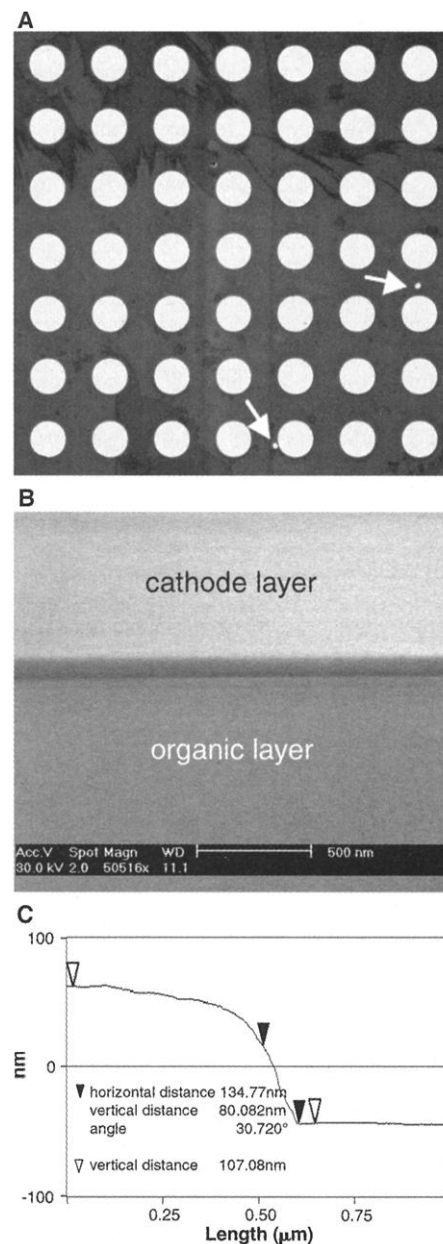

Fig. 2. (A) Optical micrograph of an array of 230-μm-diameter Mg:Ag contacts patterned by cold-welding followed by cathode lift-off. (B) Scanning electron micrograph (SEM) of the edge of a 12-μm-wide stripe showing a clearly defined nearly featureless layer pattern. (C) AFM scan taken perpendicular to the edge in (B).

defined, even over the raised surface. The metal has been removed on the right side of Fig. 4B. Both the ITO and SiO_2 surfaces retain some residual organic material. Nevertheless, the stamp was equally effective in removing metal from the region coated by ITO, SiO_2, and a combination of these layers because of deformation of the substrate under pressure. In Fig. 4C, we show an array of pixels (top), as well as

the detail of a single pixel addressed to indicate the operation of the passive matrix display (bottom).

The cold-weld technique has several advantages over previously reported patterning methods. First, it is potentially cost-effective, since the stamps are reusable after the metal layers are removed by chemical dissolution. Second, this technique offers high throughput, since the

entire electrode area of the circuit is patterned in a single step after all the layers are deposited (20). Indeed, because of its capability for very high pattern resolution, this method is especially suited for the fabrication of micro-displays. Third, roll-to-roll fabrication processes that use flexible plastic substrates can employ this technique, using stamps with patterns on the outer surface of a cylinder. Finally, although we demonstrated the fabrication of small molecular weight, vacuum-deposited OLEDs, we believe that this technique is also applicable to polymer devices where in situ shadow-mask methods are not applicable.

In summary, we demonstrated micropatterning of organic optoelectronic devices by the process of cold-welding of metal cathodes followed by lift-off from the organic substrate. Patterns were obtained with feature sizes of 12 μm and with submicrometer feature definition. Further, the method was employed to achieve a monochrome passive matrix OLED display with individually addressable pixels. This technique is potentially cost-effective, offers high throughput, and is suited for large-area and roll-to-roll fabrication.

Fig. 3. Current density versus voltage characteristic of 1-mm-diameter OLEDs patterned by cold-welding followed by cathode lift-off, compared to those prepared with conventional shadow-mask techniques. V_{10} is defined as the operating voltage corresponding to a current density of 10 mA/cm². (Inset) External quantum efficiency versus current density for the same devices.
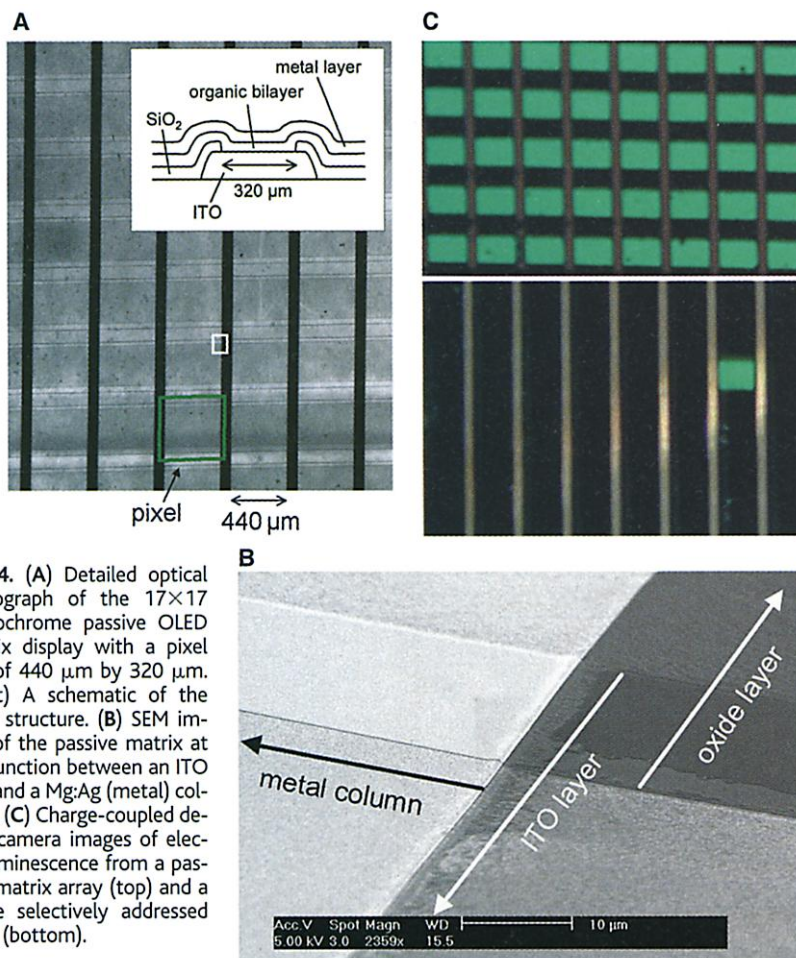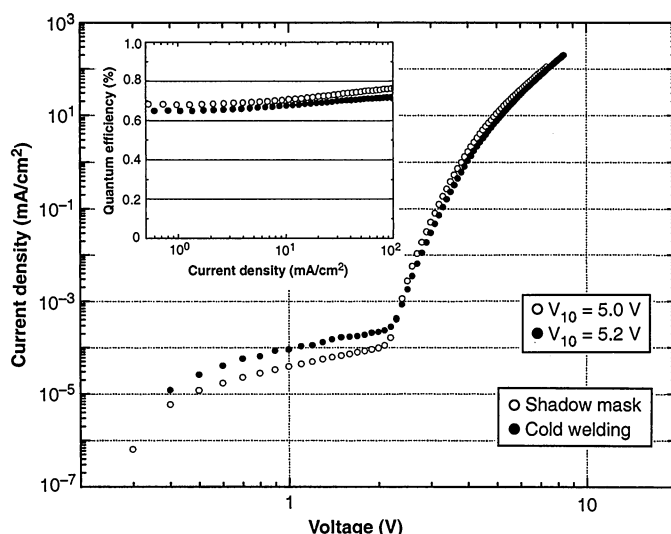

Fig. 4. (A) Detailed optical micrograph of the 17×17 monochrome passive OLED matrix display with a pixel size of 440 μm by 320 μm. (Inset) A schematic of the layer structure. (B) SEM image of the passive matrix at the junction between an ITO row and a Mg:Ag (metal) column. (C) Charge-coupled device camera images of electroluminescence from a passive matrix array (top) and a single selectively addressed pixel (bottom).

References and Notes

1. P. E. Burrows et al., J. Appl. Phys. **79**, 7991 (1996).
2. S. Miyaguchi et al., in Proceedings of the 9th International Workshop on Inorganic and Organic Electroluminescence, 14 to 17 September 1998, Bend, OR, p. 137.
3. S. Noach et al., Appl. Phys. Lett. **69**, 3650 (1996).
4. T. R. Hebner, C. C. Wu, D. Marcy, M. H. Lu, J. C. Sturm, Appl. Phys. Lett. **72**, 519 (1998).
5. J. Bharathan and Y. Yang, Appl. Phys. Lett. **72**, 2660 (1998).
6. S. C. Chang et al., Adv. Mater. **11**, 734 (1999).
7. P. F. Tian, P. E. Burrows, S. R. Forrest, Appl. Phys. Lett. **71**, 3197 (1997).
8. C. T. H. Liedenbaum et al., in 2nd International Conference on Electroluminescence of Molecular Materials and Related Phenomena, 13 to 15 May 1999, Sheffield, UK, p. Th 6.
9. D. C. Duffy, R. J. Jackman, K. M. Vaeth, K. F. Jensen, G. M. Whitesides, Adv. Mater. **11**, 546 (1999).
10. P. A. Taylor, J. S. Nelson, B. W. Dodson, Phys. Rev. B **44**, 5834 (1991).
11. J. R. Smith, G. Bozzolo, A. Banerjea, J. Ferrante, Phys. Rev. Lett. **63**, 1269 (1989).
12. F. P. Bowden and D. Tabor, The Friction and Lubrication of Solids, Part II (Clarendon, Oxford, 1964).
13. G. S. Ferguson, M. K. Chaudhury, G. B. Sigal, G. M. Whitesides, Science **253**, 776 (1991).
14. D. A. Spence, Proc. Camb. Philos. Soc. **73**, 249 (1973).
15. R. E. Bolz and G. L. Tuve, Eds., Handbook of Tables for Applied Engineering Science (CRC Press, Cleveland, OH, 1973).
16. N. P. Bansal and R. H. Doremus, Handbook of Glass Properties (Academic Press, New York, 1986).
17. E. S. Machlin and W. R. Yankee, J. Appl. Phys. **25**, 576 (1954).
18. C. W. Tang, S. A. VanSlyke, C. H. Chen, J. Appl. Phys. **65**, 3610 (1989).
19. G. Gu et al., J. Appl. Phys. **86**, 4067 (1999).
20. Further development may be necessary for devices with lateral structure (e.g., a thin-film transistor) where an electrode must be patterned without damaging the underlying organic layers.
21. We thank B. S. H. Royce for assistance in using an Instron Dynamic Testing System and Z. Suo for helpful discussions. We also thank the Defense Advanced Research Projects Agency and Universal Display Corporation for support of this work.

12 January 2000; accepted 15 March 2000